Instability of Cobalt-Substituted Polyoxometalates during the Oxygen Evolution Reaction: An Operando X-ray Absorption Spectroscopy Study

Benjamin Rotonnelli, Benedikt Lassalle-Kaiser, Antoine Bonnefont, Séverine Renaudineau, Delphine Garnier, Anna Proust, Fabrice Bournel, Jean-Jacques Gallet, Tristan Asset, Elena Savinova

Instability of Cobalt-Substituted Polyoxometalates during the Oxygen Evolution Reaction: an *Operando* X-Ray Absorption Spectroscopy Study

Benjamin Rotonnelli [1], Benedikt Lassalle-Kaiser [2], Antoine Bonnefont [3], Séverine Renaudineau [4], Delphine Garnier [5], Anna Proust [4], Fabrice Bournel [2,6], Jean-Jacques Gallet [2,6], Tristan Asset [1,*], Elena Savinova [1,*]

[1] ICPEES, UMR 7515 CNRS-ECPM-Université de Strasbourg, 25, rue Becquerel ,67087, Strasbourg Cedex 2, France

[2] Synchrotron SOLEIL, L'Orme des Merisiers, Route départementale 128, 91190, Saint-Aubin, France

[3] LEPMI, UMR 5279 CNRS-Grenoble INP-Université Grenoble-Alpes, 1130 rue de la Piscine , 38402 ST MARTIN D HERES CEDEX, France

[4] Sorbonne Université, CNRS, Institut Parisien de Chimie Moléculaire, IPCM, 75005 Paris, France

[5] CBST, UMR7199 CNRS-Université de Strasbourg et PCBIS, UAR 3286 CNRS-Université de Strasbourg, 300 Bld Sébastien Brant, CS 10413,67412 Illkirch Cedex, France

[6] Sorbonne Université, CNRS, Laboratoire de Chimie Physique Matière et Rayonnement (LCPMR), 4 place Jussieu, 75005 Paris, France

Corresponding authors: Tristan Asset, t.asset@unistra.fr ; Elena Savinova, elena.savinova@unistra.fr

Abstract

Complexes of cobalt(II) stabilised by lacunary polyoxometalates (CoPOMs) are highly discussed water oxidation catalysts (WOC). While their activity and stability in the oxygen evolution reaction (OER) have been widely explored, there is still no consensus between those claiming that CoPOMs are active and stable OER catalysts and those suggesting that they rather act as pre-catalysts, which degrade into OER-active heterogeneous CoO_x catalysts. In this work, we use *operando* X-Ray Absorption Spectroscopy along with electrochemical methods (cyclic voltammetry, chronoamperometry) to assess the activity and stability of $[Co_9(H_2O)_6(OH)_3(HPO_4)_2(PW_9O_{34})_3]^{16-}$ (Co_9POM) under chemical and electrochemical operating conditions. First, we demonstrate that Co_9POM dissolved in a phosphate buffer quickly degrades during an electrochemical OER, leaving a Co(III)/Co(II)-containing layer on the electrode surface that acts as a heterogeneous OER catalyst. This degradation is detected using both *post mortem* and *operando* X-Ray absorption near edge structure/extended X-Ray absorption fine structure. Then, the electrochemical OER is studied in the presence of 2,2'−bipyridine, which is used to eliminate Co^{2+} aqua-complexes resulting from the Co_9POM

dissociation equilibrium. Yet, this does not avoid the formation of a Co-containing precipitate, albeit of a different composition. Finally, to differentiate between degradation associated with the catalytic cycle itself and the one provoked by local pH changes in the vicinity of the electrode during the OER, the Co_9POM is studied as a homogeneous WOC with NaClO as a chemical oxidant. An irreversible loss of Co from the Co_9POM is detected after the addition of two NaClO equivalents per Co ion. These combined insights provide clear *operando* evidence of the **Co_9POM instability** under either electrochemical OER or chemical WOC operating conditions.

Graphical abstract:

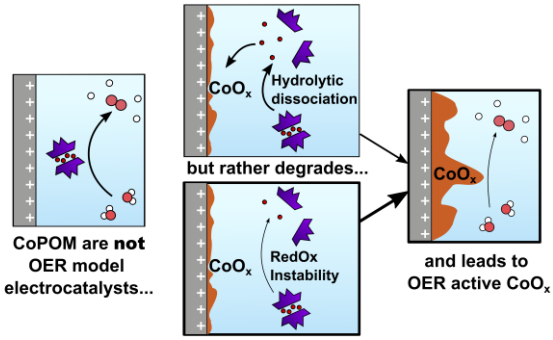

Key Words: Cobalt(II) Polyoxometalates, Oxygen Evolution Reaction, *Operando* study, X-Ray Absorption Near Edge Structure (XANES), Extended X-Ray Absorption Fine Structure (EXAFS), Stability.

1. Introduction

Aiming to deal with greenhouse gas emission and global warming, green hydrogen produced by water electrolysis is seen as a way to store and transport energy produced from renewable sources. The sluggish oxygen evolution reaction (OER) is responsible for a significant part of energy losses during water electrolysis. To this end, worldwide efforts are devoted to the development of efficient, stable and inexpensive OER catalysts. Transition metal (Co, Ni, Fe)−oxide-based heterogeneous electrocatalysts are widely studied as OER catalysts, mainly in alkaline media. Despite numerous studies, the OER mechanism is still not fully understood.[1] Contrary to heterogeneous catalysts, which comprise of a variety of active sites hindering the OER mechanistic understanding,[2,3] transition metal complexes benefit from a well-defined chemical environment around the metal centre, making them attractive model **WOC** (term furtherly used for water oxidation through chemical oxidation) and **OER** (term furtherly used for water oxidation through electrochemical oxidation) catalysts.[4]

CoPOMs, notably $[Co_4(H_2O)_2(PW_9O_{34})_2]^{10-}$ (Co_4POM) and $[Co_9(H_2O)_6(OH)_3(HPO_4)_2(PW_9O_{34})_3]^{16-}$ (Co_9POM), were proposed as catalysts for the OER in

neutral pH conditions by Hill *et al.* [5] and Galan-Mascaros *et al.* [6] (*cf.* **Figure 1.A,B**), and since then have been studied by several research groups, provoking significant controversies. Contrary to heterogeneous electrocatalysts, which are usually deposited on the surface of an inert (e.g. glassy carbon) working electrode, CoPOM are molecular water-soluble species and were studied being dissolved in the electrolyte in the first place. They were investigated either under chemical water oxidation conditions using $[Ru(bpy)_3]^{3+}$ or NaClO as oxidants or OER conditions by dissolving them in phosphate or borate buffer electrolytes and using glassy carbon (GC) as a working electrode. While the activity of CoPOMs as a homogeneous WOC under chemical water oxidation conditions has been widely recognised,[7] studies of the OER quickly revealed their degradation and formation of a CoO_x layer (detected with *post mortem* analyses, **Figure 1.C**) on the working electrode.[6,8–10] The degradation has been attributed to an unavoidable Co^{2+}_{aq} leaching from the CoPOM complexes due to their hydrolytic dissociation in aqueous media (*cf.* **equation 1**), followed by formation of a CoO_x layer during the OER.[11,12] The deposition of the CoO_x layer on the electrode surface and its high electrocatalytic activity were confirmed by performing the OER in a Co^{2+}_{aq} – containing solution.[13,14] Hence, the formation of the CoO_x layer, which is highly active towards the OER, in CoPOM-containing systems, quickly lead to the question: "Are CoPOMs true OER electrocatalysts or only pre-catalysts?" that is debated ever since.

$$Co_nPOM + y.H_2O = [Co(H_2O)_y] + Co_{n-1}POM \quad \textbf{(Eq. 1)}$$

While it appeared to be difficult to totally deny CoPOMs as homogeneous OER electrocatalysts, some studies proved that a small concentration of leached $Co^{2+}_{(aq)}$ could account for the OER activity of CoPOM in the electrolyte.[11] In an attempt to delineate the OER currents arising either from CoPOM or from the CoO_x catalysts, 2,2'-bipyridine (bpy) was used as a chelating agent, complexing Co^{2+}_{aq} into an OER-inactive $[Co(bpy)_3]^{2+}$ species. Several studies reported that despite an addition of the bpy ligand, a certain OER activity was still retained suggesting that CoPOM itself could be OER-active.[5,6,15]

In this work, we apply X-ray absorption spectroscopy (X-ray absorption near edge structure, XANES and extended X-ray absorption fine structure, EXAFS) to study Co_9POM first *post mortem* and then *operando* under water oxidation conditions, in order to assess its (in)stability. The experiments are performed with Co_9POM dissolved in an aqueous electrolyte to clarify its ability to act as a homogeneous molecular catalyst. Measurements are carried out in highly concentrated phosphate buffer (pH=6.0), to mitigate the local pH modification as much as possible.[6,7,9,10,16] Indeed, the OER (*cf.* **equation 2**):

$$2H_2O = O_2 + 4H^+ + 4e^- \quad \textbf{(Eq. 2)}$$

can lead to a decrease of the local pH in the vicinity of the working electrode. Meanwhile, lacunary polyoxometalates are known to lose their propensity to complex Co^{2+} at low pH due to their condensation into various degradation products. [17]

In order to distinguish between the Co_9POM degradation induced by either local electrolyte acidification or changes in the Co coordination and oxidation state during the catalytic cycle, measurements are performed either in the electrochemical (OER with GC as an anode) or in a chemical mode (WOC with NaClO as a sacrificial oxidant). Furthermore, measurements are also performed with the addition of bpy as a chelating agent to delineate degradation due to the oxidation of either Co^{2+}_{aq} or Co_9POM itself.

2. Experimental

Electrochemistry

Sodium phosphate buffer (NaPi) was prepared by dilution of a 85 wt. % H_3PO_4 solution in ultrapure water (18.2 MΩ) followed by neutralisation with 50 wt. % NaOH to reach pH=6.0, which was controlled with a calibrated pH-meter. Concentrations were calculated considering the dilution effect. CoPOM solutions were freshly prepared before each experiment.

The electrochemical cell (SVC-2 BioLogic electrochemical cell setup) used was a single-wall one-compartment ~10 mL glass cell carefully washed my immersion in caroic acid, and rinsed in ultrapure-water prior to electrolyte addition. The system was immersed in thermostated bath at 25°C and degassed with N_2 during t > 10 min prior to each measurement. The cell was equipped with three electrodes. A 5 mm diameter-rod glassy carbon (GC) electrode, polished by alumina (1 µm → 0.3 µm → 0.05 µm) and sequentially sonicated for 5 minutes in acetone, absolute ethanol, and water was used as a working electrode (WE). The WE-rod was wrapped in a Teflon tape to avoid electrolyte contact with its sides. A flame-annealed Pt wire served as a counter electrode (CE), and a K_2SO_4-saturated mercury/mercurous sulphate electrode, $Hg/HgO/K_2SO_4$ (saturated aqueous solution) was used as a reference electrode (RE). The RE was calibrated against reversible hydrogen electrode (RHE) in the same electrolyte batch and temperature conditions, using a platinised Pt reference hydrogen electrode under direct H_2 bubbling, prior to experiment. Electrochemical measurements (chronoamperometry and cyclic voltammetry) were performed using Gamry Ref 600 potentiostat.

Blank CVs (i.e. catalyst-free) were systematically carried out prior to catalyst addition to the system, using the same electrolyte batch, in order to verify system's cleanliness and to compare the activity with and without CoxPOM catalyst.

CoPOM synthesis and characterisation

Co_4POM and Co_9POM used in this work were synthesised at the *Institut Parisien de Chimie Moléculaire* (Sorbonne Université, Paris, France) following an optimised method inspired by Refs. [18,19] and described in the **supplementary information** (SI). The purity of each product was verified using IR-spectroscopy and ^{31}P-NMR spectroscopy before use (see **Figure S1-3**). Since recording and analysis of

NMR data of paramagnetic compounds is less common than for diamagnetic ones,[20] the challenges and experimental methods employed are presented in the **SI**.

X-Ray Absorption spectro-electrochemical cell

Ex situ, in situ and *operando* XANES measurements shown in the main text of this article were performed at the LUCIA beamline [21] of synchrotron SOLEIL, with a ring current of 500 mA and a nominal energy of 2.3 GeV. The beamline energy is selected by means of a Si(111) double-crystal monochromator and the beam size is 2 x 2 mm^2. The data were collected in fluorescence yield mode with a single-channel silicon drift detector from Bruker. Data reduction, normalisation, and Fourier-Transforms were performed with the Athena software.[22] All data were normalised to the intensity of the incident beam. The spectroelectrochemical cell, described elsewhere,[23] and shown in **Figure S6** is composed of a 0.06 mm x 6 mm x 2 mm GC working electrode, a Pt plate CE and a silver wire floating RE. Electrodes were carefully washed by successive sonication in acetone, absolute ethanol and water, 5 min each. The potential calibration was performed using the quinone/hydroquinone (Q/HQ, redox couple present on the natively oxidized glassy carbon electrode) peak as an internal reference (E(Q/HQ)=0.657 V *vs*. RHE at pH=6.0).[24] As this method of calibration can result in some uncertainties, the potential corrected with this method will be referred as "*vs.* RHE*****".During the measurements, the electrolyte was continuously circulated in a closed loop with a peristaltic pump, to and from an electrolyte container of 5 mL. XANES spectra of reference compounds were collected as boron nitride pellets with a 10 wt.% dilution. The acquisition parameters of the "stepscan" mode were defined depending on the spectral region following the **Table 1** acquisition time. "Quick" spectra were recorded in "flyscan mode" *i.e.* continuous scan of the incident beam energy. Spectra were recorded in the [7620,7900] eV range, 1 point every 0.3 eV, with a collection time of 200 ms per point.

Table 1: "Stepscan" mode acquisition parameters used in the work

Energy range / eV	[7620,7700]	[7700,7740]	[7740,7800]	[7800,7900]	[7900,8100]
Step size / eV	2	0.2	0.5	1	2
Acquisition time / s	2	2	5	4	8

CoPOM chemical oxidation

A 1 mM Co_9POM solution in 0.72 M NaPi at pH=7.0 was obtained by direct dilution of Co_9POM into the desired electrolyte. In parallel, a 100 mM NaClO solution in 0.72 M NaPi at pH=7.0 was prepared by: (i) neutralisation of a 50 wt. % NaClO solution with NaPi (pH=4.0), up to pH=7.0 and (ii) dilution of the obtained intermediate solution by 0.72 M NaPi with pH=7.0. *Operando* chemical oxidation analysis was performed by successive addition of the desired amount of the solution containing 100 mM of NaClO into the 1 mM Co_9POM in NaPi 0.72 M solution. XANES spectra were recorded in the "quick" mode immediately after each addition of the NaClO solution aliquot (3 scans, 3'30'' per scan), and then in the

"stepscan" mode (2 scans; 40 minutes per scan). The difference of pH between the chemical oxidation and the electrochemical oxidation experiments was chosen to match the pH conditions used in Galan-Mascaros *et al.* work [6]. As the pH stability range of Co_9POM is estimated between pH 5.5 and 11.0, this slight pH increase is not expected to cause a problem.[25,26] Further discussion on pH=7 system is brought in SI section SI-6.

3. Results and Discussion

3.1. Electrochemical study of the CoPOM's stability

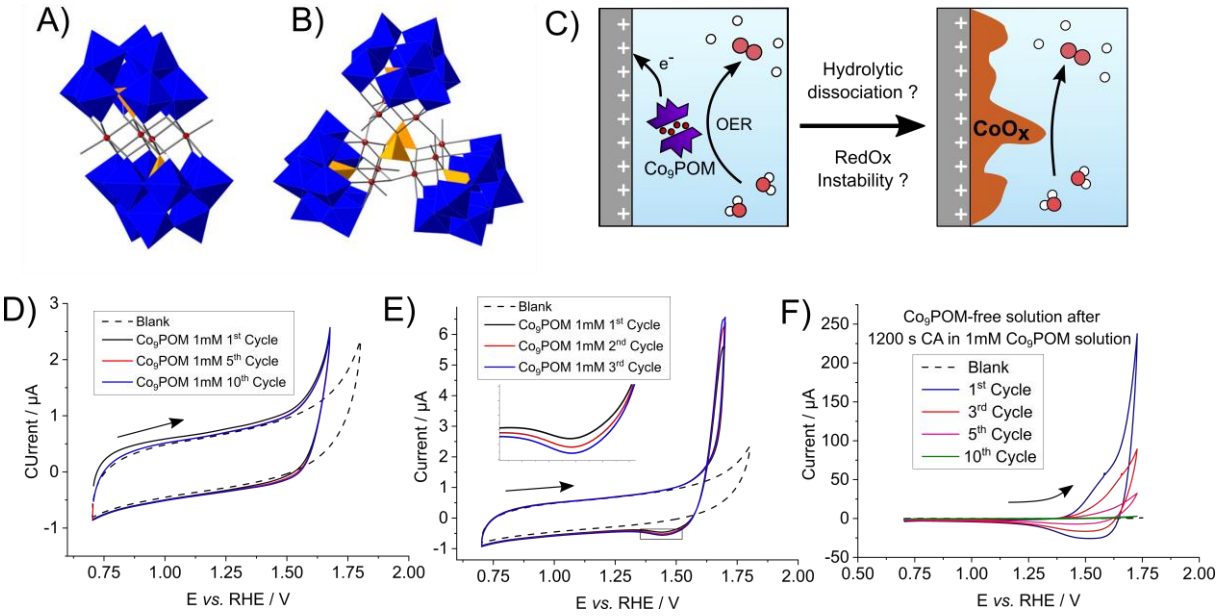

Figure 1: (**A**) and (**B**) Ball and stick model of Co_4POM and Co_9POM respective representations, Co(II) is red, with pending sticks showing coordination sites where H_2O molecules bind, PO_4 - yellow tetrahedra (with P in the center), WO_6 – blue octahedra (with W in the center). Adapted with permission from Ref.[11] Copyright 2024 American Chemical Society. (**C**) Illustration of the CoPOM electrocatalytic system that moves from an homogeneous catalytic reaction, through an heterogeneous catalytic reaction through the formation of CoOx layer on the working electrode. (**D**, **E**, **F**) CVs recorded of a GC electrode in a 0.72 M NaPi buffer solution (pH=6.0) in the presence (**D**, **E**) or in the absence (**F**) of 1 mM Co_9POM in the electrolyte in the potential interval from 0.7 to 1.7 V *vs*. RHE (**D**) or 0.7 to 1.725 V *vs*. RHE (**E**,**F**). CVs in panel (**F**) shows the electrochemical behaviour of the GC working electrode in CoPOM-free electrolyte (0.72 M NaPi buffer at pH=6) after a 1200 s chronoamperometry at 1.6 V *vs*. RHE in 1 mM Co_9POM electrolyte (*cf*. **Figure S4.A**). Similar analyses are carried out for Co_4POM and shown on **Figure S4**.

The stability of the Co_4POM and Co_9POM (displayed on **Figure 1.A,B**) during the electrochemical OER was studied with cyclic voltammetry (CV) and chronoamperometry (CA) followed by *post mortem* XANES characterisation of the working electrode (WE) to detect possible Co-containing precipitates. **Figure 1.D,E** shows sequential CV cycles applied to a GC electrode in a 1 mM Co_9POM solution in different potential intervals: first between 0.7 and 1.7 V *vs.* RHE

(**C**), and then between 0.7 and 1.725 V *vs*. RHE (**D**). The OER manifests itself by the current increase above ~1.5 V *vs*. RHE, and the CVs in **Figure 1.D** are reproducible, thus testifying in favour of the Co_9POM stability at potentials below 1.7 V *vs*. RHE. However, even a slight increase of the electrode potential to 1.725 V *vs*. RHE (**Figure 1.E**) results in a qualitative change of the behaviour: the anodic currents increase in sequential CV cycles, and a cathodic peak at 1.45 V *vs*. RHE appears in the negative scan, that can be attributed to Co(IV)/Co(III) redox transition [14,27,28] suggesting precipitation of a Co-containing layer on the GC surface. To verify whether the CoPOM stability is related to the applied potential or rather to the number of imposed catalytic cycles (and hence the amount of transferred charge), constant-potential CA measurements were performed at 1.6 V *vs*. RHE (*i.e.,* lower potential) for 20 min (see **Figure S4.A**). The analysis reveals an increase in the current for Co_9POM as early as after ~10 sec of electrolysis suggesting degradation of the complex and eventually formation of a heterogeneous Co-containing layer on the electrode surface as confirmed in what follows. The WE was then transferred in an electrochemical cell filled with a Co_9POM-free NaPi buffer solution. The significantly higher anodic currents (compared to the pristine GC electrode, see **Figure 1.F**) along with the appearance of the anodic and cathodic peaks typical for redox processes of Co oxides, both testify in favour of a Co oxide layer deposition during the OER in a Co_9POM solution, and prove that the degradation is not directly related to the electrode potential but rather to the amount of charge transferred (and thus number of catalytic cycles). Note that continuous decrease of the currents revealed by repetitive CV cycles in the Co_9POM-free NaPi buffer is in agreement with the Pourbaix diagram of Co pointing to solubility of Co(II) (hydr)oxide at pH≤6.[29] Similar results were observed for Co_4POM, albeit current increase during the CA was less abrupt (see **Figure S4**).

Post mortem analyses of a GC electrode exposed to similar operational conditions by transmission electron microscopy-energy dispersive X-ray spectroscopy (TEM-EDX), XANES at the Co L-edge and X-ray photoelectron spectroscopy, XPS (see **Figure S5** and associated discussion) reveal an amorphous, inhomogeneous Co− and O−containing layer on the surface. The extremely low tungsten fraction in this layer let us conclude that electrolysis of CoPOM solution leads to the formation of a CoO_x degradation layer. This conclusion agrees with that of Stracke *et al.* who studied Co_4POM albeit under much harsher conditions (1.9 V *vs.* RHE).[8] This CoO_x degradation layer could result either from (i) CoPOM metal-ligand dissociation equilibrium (Eq. 1) and hence non-zero concentration of $Co^{2+}_{(aq)}$ leached in solution, or (ii) CoPOM degradation due to the local acidification resulting from the OER, or (iii) CoPOM instability resulting from the cobalt oxidation and change of coordination as part of the catalytic cycle. To differentiate between these options and eventually shed light on the changes of the oxidation

state and local chemical environment of Co during the catalytic cycle, *operando* XANES measurements were performed under different operation conditions.

3.2. Operando XANES study of CoPOMs during the electrochemical OER

Operando XANES spectra at the Co K-Edge were collected for a Co_9POM solution with different potentials applied to the GC working electrode. We note that the shape of the CV (**Figure 2.A**) collected in the spectroelectrochemical cell is similar to the one obtained in a three-electrode electrochemical cell, albeit with higher intensity of the quinone/hydroquinone redox transition around ~0.66 V *vs.* RHE* arising from the glassy carbon foil (cathodic peak position: E_{cat}= 0.645 V, anodic peak position: E_{an}= 0.685 V).[24] *This redox peak was used to calculate the potential of the reference electrode of the system, a floating Ag wire. Hence, the conversion of the potential into the RHE scale may not be precise and will be referred as RHE**.

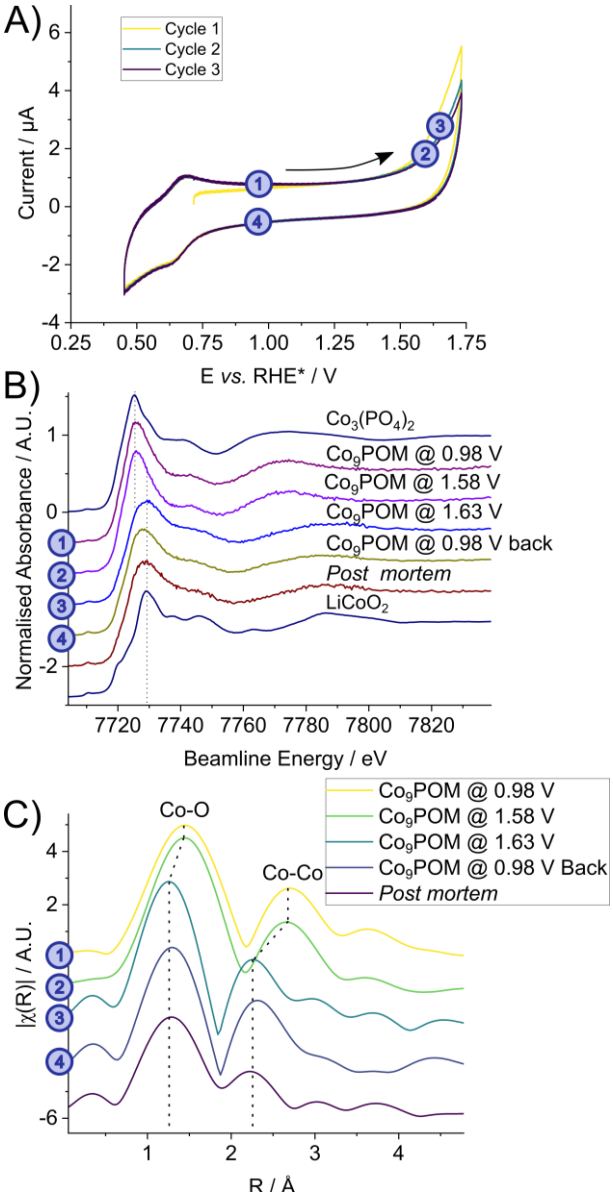

Figure 2: A) CVs in the spectro-electrochemical cell with 1 mM Co_9POM in 0.72 M NaPi buffer (pH=6.0), at 100 mV/s. The counter electrode is a Pt foil, the working electrode is a glassy carbon foil, also acting as a window for the spectra recording, and a Ag wire is used as a floating reference electrode. The potentials **1**: 0.98 V, **2**: 1.58 V, **3**: 1.63 V, and **4**: back at 0.98V *vs.* RHE, at which the *operando* spectroscopic data were recorded are reported directly on the curve. **B)** *Operando* Co K-Edge XANES spectra and the **C)** corresponding FT-EXAFS spectra collected at the specified potentials. The spectra of the $Co(II)_3(PO_4)_2$ and $LiCo(III)O_2$ references are shown for comparison. **P*ost mortem*** designates the signal collected after the replacement of the electrolyte in the spectroelectrochemical cell by ultra-pure water without opening the cell.

Co K-Edge spectra were recorded at the open-circuit potential (OCP~0.98 V *vs*. RHE^*), at the OER 'onset' at 1.58 V, during the OER at 1.63 V (as illustrated by **Figure 2.A**) as well as *Post mortem* after flushing the spectro-electrochemical cell with ultra-pure water. The spectra are shown in **Figure 2.B**, and the associated FT-EXAFS spectra in **Figure 2.C**.

Neither K-Edge Co spectra in **Figure 2.B** nor FT-EXAFS spectra in **Figure 2.C** show noticeable changes when the potential of the WE is increased from 0.98 V to 1.58 V. This implies that no degradation of the Co_9POM is observed under these conditions.

When the electrode potential is increased to 1.63 V, a strong shift in the Co K-edge white line is observed (**Figure 2.B**). While the XAS Co K-edge spectra taken at the OCP and at the OER onset are similar to the Co(II) reference ($Co_3(PO_4)_2$), the spectrum taken at 1.63 V is closer to the Co(III) reference ($LiCoO_2$), as confirmed by the white line position and the half-edge jump energy position (**Figure 2.B** inset window), suggesting that Co(II) is oxidised into Co(III) in the OER potential range. These changes are accompanied by shortening of the Co-O (from 1.45 Å to 1.25 Å) and Co-Co (from 2.67 Å to 2.25 Å) apparent distances highlighted from the FT-EXAFS spectra (**Figure 2.C**) which is consistent with the reduction of the bond length and/or modifications in the Co coordination sphere due to the oxidation of Co(II).[30] These changes are irreversible since stepping back to the OCP does not allow one to restore the initial spectrum.

Similarly to what was observed in the conventional electrochemical cell (**Figure 1.C,D**), one may assume that Co_9POM degrades during the electrolysis leaving behind a Co-containing precipitate on the GCE surface. To prove this, a XANES Co K-Edge spectrum was measured *post mortem* after removing the electrolyte from the spectro-electrochemical cell and filling the latter with ultra-pure water without opening the cell and exposing it to the ambient atmosphere. The *post mortem* spectrum confirms formation of an oxide layer consisting of Co(III) (**Figure 2.B,C**) in agreement with *ex situ* findings reported in the literature.[6,11] Furthermore, an increase of the Co K-Edge intensity is observed on the non-normalised XANES spectra shown in **Figure S7.A.** Specifically, at 1.63 V, the edge absorbance intensity is increasing, which supports accumulation of a CoO_x layer on the electrode. Back at 0.98 V, the edge absorbance intensity decreases, *i.e.* the CoO_x layer dissolves, similarly to what was observed in **Figure 1.E** and **S4.D**. Those changes are both observable on the overall spectra intensity, and the spectra background (>7800 eV region), as the electrodeposition/dissolution of the CoO_x layer on the GC electrode is a time-dependent process, and each spectrum took about 20 minutes to be recorded.

Considering the similarities between the *post mortem* XANES spectrum and the one taken under OER conditions (at 1.63 V *vs*. RHE), we conclude that the Co_9POM is degrading under the OER conditions, (despite the OER current being relatively small) and that the Co(III) degradation product deposited on the WE dominates the spectrum.

3.3. *Operando XANES study of CoPOMs during the electrochemical OER in the presence of bpy*

As mentioned in the introduction, previous studies suggested that the $Co(III)O_x$ layer during the OER could arise from the electrooxidation of Co^{2+}_{aq} leached in solution due to CoPOM dissociation equilibria (potentially impacted by the local pH modification during the OER).[11] To check this hypothesis, we followed an approach previously described in the literature, which consists in the addition of 2,2'-bipyridine (bpy) to a CoPOM solution.[5,6] The idea is to shift the equilibrium and transform any Co^{2+}_{aq} present in solution into $[Co(bpy)_3]^{2+}$, which is believed to be inactive towards the OER.[5] To this end, the conditions of the experiment described in **section 3.2** and presented in **Figure 2** were modified by adding three bpy equivalents per Co atom (27 eq. per Co_9POM). The two sets of data were then compared (see **Figure 3**) to determine if the cobalt oxidation can be observed without degradation as a proof of the CoPOM stability and reactivity under the OER conditions.

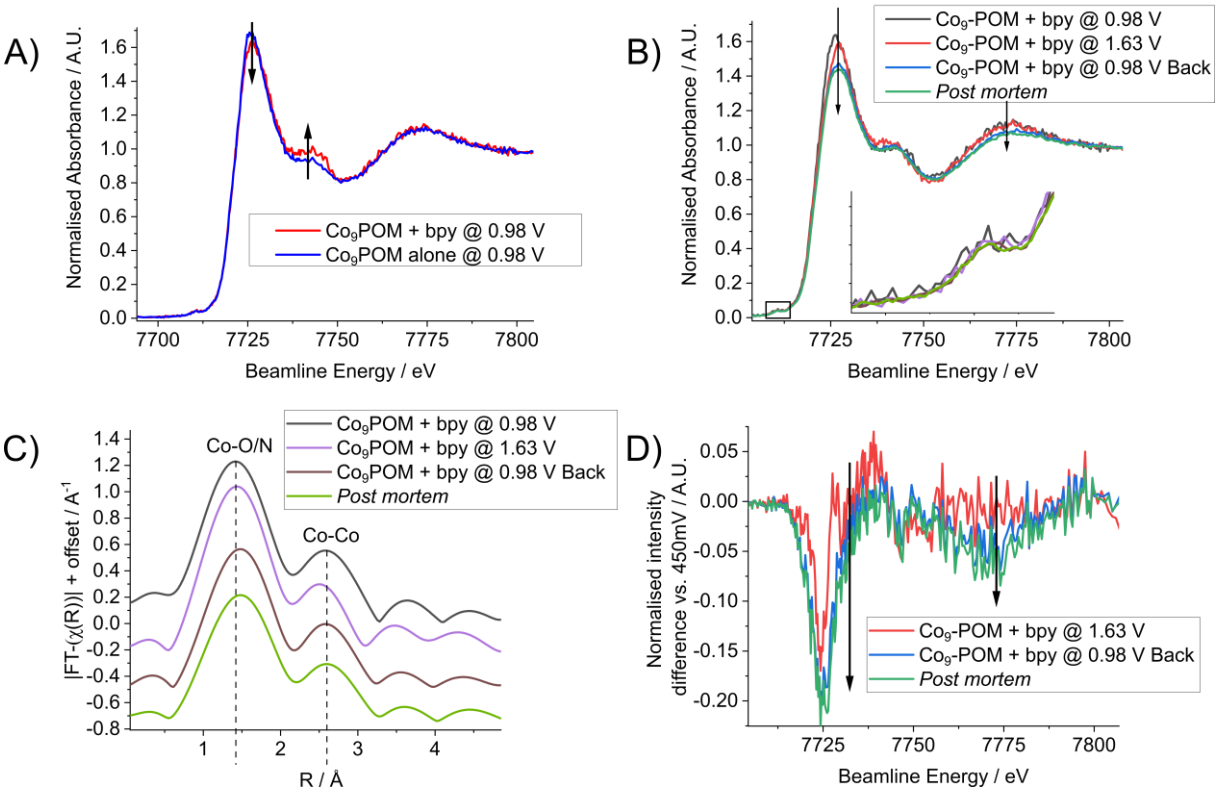

Figure 3: *Operando* measurements of 1 mM Co_9POM in 0.72 M NaPi buffer (pH=6.0) in the presence of 27 mM bipyridine (3 eq. per Co). **A)** comparison of XANES Co K-Edge spectra at the open circuit potential, OCP (1.20 V *vs.* RHE) in the presence and in the absence of bpy. **B)** Co K-Edge XANES spectra and **C)** corresponding FT-EXAFS spectra collected in the presence of bpy at potentials indicated in the legend. **D)** Difference XANES spectra obtained by subtraction of the initial spectrum at 0.98 V *vs. RHE* from spectra shown in figure B) at 1.63 V, 0.98 V back and *post mortem*. The *post mortem* spectrum

was measured after the replacement of the electrolyte in the spectroelectrochemical cell by ultra-pure water without opening the cell.

Firstly, the XANES fingerprints between the Co_9POM solution alone and Co_9POM+bpy solutions are compared at 0.98 V *vs*. RHE* (**Figure 3**.**A**). While the general shape of the XANES spectra is retained and does not highlight any change in the cobalt oxidation degree, the white line and the maximum at 7743 eV evolved, suggesting that bpy influences the local environment of cobalt cations. This can be explained by the expected formation of Co(II)-bpy complexes, presumably $[Co(bpy)_3]^{2+}$. Changes in the spectra can also be explained by a shift in Co-POM hydrolytic dissociation equilibria, due to the bpy present in excess, which is complexing $Co^{2+}_{(aq)}$.

We then compared the XANES spectra and the associated FT-EXAFS under *operando* conditions, shown on **Figure 3.B** and **C**. Similarly to the protocol applied in **section 3.2**, the potential is first set at the OCP (0.98 V), then increased up to 1.63 V and decreased back to 0.98 V to determine the reversibility of the system. A *post mortem* characterisation of the WE surface by the replacement of the electrolyte by ultrapure water is also performed. One can observe that regardless of the potential applied on the system, the white line position is slightly increasing towards higher energies (7726 eV to 7727 eV), while its intensity slightly decreased as well as the maximum intensity of the 7773 eV peak (**Figure 3.D**). Those observations are hinting at an irreversible change in the structure of the Co-containing species and is further supported by the visual observation of the formation of a beige precipitate in the solution. The intense Co K-edge signal in the *post mortem* spectra (**Figure S7.A)** confirms the presence of an insoluble Co-containing species on the electrode surface. Therefore, we can conclude that an insoluble species is formed during the measurements and eventually dominates the Co-K edge signal. $[Co(bpy)_3]^{2+}$ has good solubility in water [31] and no precipitation was reported in the literature following the addition of bpy in CoPOM solutions.[5,6] Hence, the precipitate was not ascribed to $[Co(bpy)_3]^{2+}$. However, it was reported in literature that the bpy ligands can link to Co(II) directly from cobalt-polyoxometalates complexes to form new complexes or organic-inorganic polymers,[32,33] which is consistent with the lack of strong changes in relative intensity of the EXAFS peak corresponding to a Co-Co interaction (*i.e.,* this indicates that CoPOM-derivatives are present in the precipitate). This assumption is confirmed by XPS elemental analysis *post mortem* (**figure S7.C**), which indicates the precipitate is composed of N (16 %), Co (6 %) and W (8 %). As the Co/W ratio does not match the Co_9POM theoretical composition (**Figure S5.C**), the precipitate is therefore a solid formed from bpy and CoPOM degradation products. From these observations, it appears that bpy greatly impacts the Co_9POM transformations during the OER. It does prevent the formation of the cobalt(III) oxide layer on the working electrode, instead leading to the precipitation of a Co(II)-bpy-POM species. This indicates that the bpy

addition does not avoid the degradation process, but rather changes the chemistry of the final degradation product. But the question still remains, 'Does the Co-POM degradation arise from the local pH variation during the OER or is it induced by an intrinsic instability of the Co-POM during the catalytic cycle?'. We attempt to answer this question in the next section.

3.4. Operando XANES study of the CoPOM during the chemical OER

Local pH changes are strongly tied to the OER, where the reaction occurs close the electrode/electrolyte interface, where the charge transfer from Co-POM to the GC occurs.[34,35] Hence, in this section we study the homogeneous WOC in the presence of Co_9POM and a sacrificial chemical oxidant. As the WOC is occurring in the solution bulk rather than being localised near the electrode/electrolyte interface, the pH modification resulting from the water oxidation is mitigated more efficiently by the buffer. To this end, we used NaClO as an oxidant, similarly to previous studies addressing the Co_9POM activity for the chemical oxidation of water [6,36]. Here, *operando* XANES is used to assess the stability of Co_9POM depending on the number of oxidising equivalents (*i.e.,* 0, 1, 2, 4 and 8) of NaClO per Co atom (which corresponds to 0, 9, 18, 36 and 72 mM of NaClO added in total). Two types of spectral acquisitions were used: 'quick' XANES, to detect Co oxidation immediately after the addition of NaClO (*i.e.* 3 scans of 3.5 min each), followed by a 'stepscan' XANES (*i.e.* 2 scans of 40 min each) to obtain more precise information regarding the oxidation state and local environment of Co after the catalytic cycle.

The results are presented in **Figure 4**. Regardless the number of NaClO equivalents, no shift in the Co K-Edge is observed during the 'quick' XANES measurements performed right after the addition of NaClO (**Figure 4.A**), *i.e.* no Co(III) or Co(IV) was observed, the latter degrading or reacting fast with water to produce O_2 and Co(II). The 'stepscan' spectra (**Figure 4.B**) obtained 30 min after the addition of NaClO show a slight change in the main Co K-Edge peak. This indicates a modification in the Co chemical environment upon addition of as little as two NaClO equivalents. The resulting FT-EXAFS (**Figure 4.C**) shows a strong decrease of the FT-EXAFS features with the increasing number of NaClO equivalents, highlighting the global loss of organisation around the cobalt cations. In addition, one may observe a slight increase of the Co K-pre-edge absorption. These changes may be tentatively attributed to the increase of the probability of a $Co_{1s} \rightarrow Co_{3d/4p}$ transition with the NaClO addition, due to the loss of the octahedral chemical environment around cobalt. The higher probability of transition would result from a stronger dipole transition character to the 3d orbital, due to a stronger 3d-4p mixing compared to pure quadripolar transition to the 3d orbitals in non-deformed octahedral environment.[37,38]

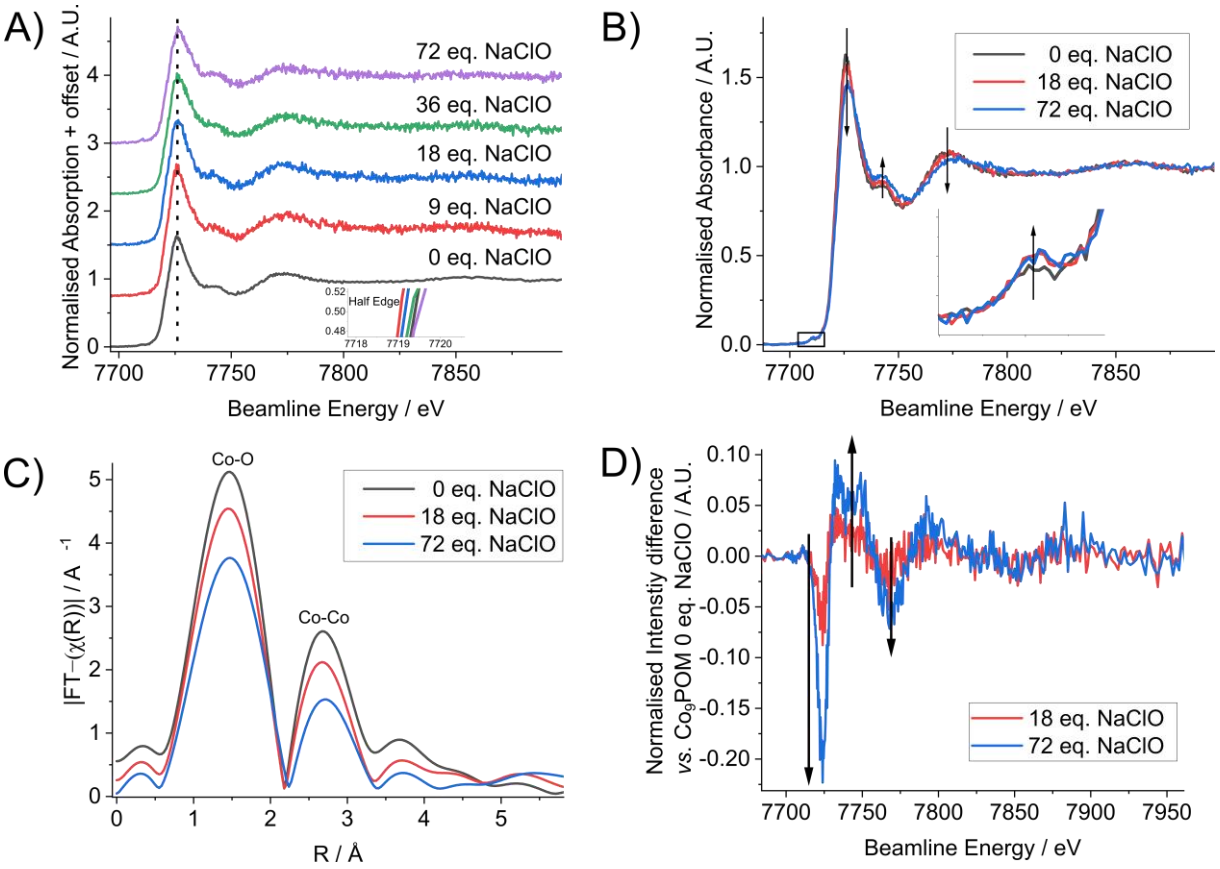

Figure 4: *Operando* XANES Co K-edge analysis after 0, 9, 18, 36 and 72 mM of NaClO added in 1mM Co_9POM solution, in phosphate buffer 0.72 M pH = 7. **A)** "Quick" XANES Co K-edge acquisition, "immediately" after the NaClO addition. **B)** "Stepscan" XANES spectra 30 min after the last NaClO addition. **C)** EXAFS Fourier Transform of the spectra presented in panel B). **D)** Differential Co-K edge spectra between the spectra shown on panel B) after 18 eq. and 72 eq. of NaClO added, *and* the initial spectrum at 1.2 V *vs*. RHE.

Overall, the changes of the XANES spectra are attributed to both (i) the loss of cobalt in Co_9POM complexes (*i.e.,* $Co_9POM \rightarrow Co_{(9-y)}POM$) and (ii) the loss of the octahedral environment. The absence of modification in the Co-O bond indicates that no bonds were formed (*e.g.,* Co-Cl – 1.94 Å apparent distance) to the detriment of the Co-O (1.61 Å apparent distance) bonds, ruling out a possible POM/chloride competition as Co complexation ligands [39]. Consequently, the Co_9POM degradation and the Co leaching arise not only from the local pH changes and hydrolytic dissociation (as discussed in **section 3.2**) but also from the water oxidation catalytic cycle itself. The results indicate that NaClO must have effectively oxidised Co-POM, but that this oxidation, or the following reduction during the H_2O oxidation is leading to an irreversible degradation of the Co_9POM structure, resulting into the formation of $Co_{(9-x)}POM$ and leached Co^{2+}_{aq}.

Further information is provided in **supporting information** (**Section SI-7, Figure S9**) on other degradation mitigation strategies, *e.g.,* use of the CoPOM in a crystalline form. Indeed, recent

works argued that CoPOMs in a solid crystalline form are more stable against pH changes and oxidation conditions.[40–43] Hence, we also investigated the Co_4POM and Co_9POM in a crystalline form in an oxidative gaseous environment, using XANES Co L-Edge *in-situ* measurements to assess changes of the oxidation state of Co and a possible degradation of the CoPOMs. The results are discussed in the supporting information.

Conclusions

To the best of our knowledge, this work is the first *operando* study of the cobalt substituted polyoxometalate Co_9POM as an OER electrocatalyst or a WOC catalyst using operando X-Ray Absorption Spectroscopy at the Co K-Edge. The catalyst is studied in homogeneous media under different oxidation conditions, firstly using OER without bpy, then in the presence of bpy in order to mitigate the influence of $Co^{2+}_{(aq)}$ on the system's stability and, finally, using WOC with NaClO as a sacrificial oxidant. Our main findings can be summarised as follows:

(i) An irreversible degradation of Co_9POM in solution, into a solid Co(III)/Co(II) oxide layer on the anode occurs during the OER. This oxide layer arises from CoPOM hydrolytic dissociation to $Co^{2+}_{(aq)}$ (which may be enhanced by local pH modifications at the electrode vicinity during the OER) followed by its precipitation on the electrode surface in the form of Co(II) oxide/hydroxide and eventual oxidation to Co(III) oxide/hydroxide in the potential interval of the OER. As this newly formed cobalt oxide layer is OER-active, the electrocatalytic system transforms from a homogeneous to a heterogeneous one.

(ii) The role of $Co^{2+}_{(aq)}$ in the system's stability can be supressed by complexation with an excess of bpy. The formation of the oxide layer is therefore avoided but another degradation product is formed under oxidation conditions, identified as a bpy−Co−POM containing solid. This indicates that addition of bpy does not avoid CoPOM degradation but rather changes the chemistry of the final degradation product;

(iii) To minimize the influence of the pH modification due to the OER at the electrode/electrolyte interface, chemical oxidation of water is attempted in the Co_9POM solution using successive additions of NaClO. The complex degrades upon the addition of as little as two NaClO equivalents per Co ion, evidenced by a global loss of organisation around Co cation.

Co_9POM is therefore shown to be unstable when exposed to oxidation conditions either in a homogeneous system (WOC) or in a heterogenous system (OER) and therefore should not be considered as a model chemical or electrochemical catalyst for the water oxidation.

Supporting information

SI-1: CoPOM synthesis and characterisation.

SI-2: Co4POM electrochemical characterisation.

SI-3: Post mortem analysis of the CoOx degradation layer.

SI-4: XAS spectro-electrochemical cell measurement used in this work.

SI-5: Operando study of Co_9POM in the presence of bipyridine.

SI-6: Discussion on CoPOM behaviour depending on pH.

SI-7: Quasi-in situ study of CoPOMs in a crystalline form.

SI-8: Summary of Co K-Edge spectra for Co_9POM collected under operando conditions.

Acknowledgments

We thank the synchrotron SOLEIL for the beamtime allocation (proposal 20220530) and financing, as well as TEMPO and LUCIA beamline staff, for their help in the collection of the XANES experimental data presented in this work. We additionally thank the ISISS beamline at BESSY II synchrotron for the data recording presented in SI (proposal 202-09905). We thank Ms. Saloua Nouma for the TEM imaging. Finally, Dr. José Ramon Galan Mascaros and Dr. Mercè Martin-Sabi are warmly acknowledged for their advice in the synthesis of Co_9POM.

References

(1) Vazhayil, A.; Vazhayal, L.; Thomas, J.; Ashok C, S.; Thomas, N. A Comprehensive Review on the Recent Developments in Transition Metal-Based Electrocatalysts for Oxygen Evolution Reaction. *Applied Surface Science Advances* **2021**, *6*, 100184.

(2) Lopes, P. P.; Chung, D. Y.; Rui, X.; Zheng, H.; He, H.; Martins, P. F. B. D.; Strmcnik, D.; Stamenkovic, V. R.; Zapol, P.; Mitchell, J. F.; ***et al.*** Dynamically Stable Active Sites from Surface Evolution of Perovskite Materials during the Oxygen Evolution Reaction. *J Am Chem Soc* **2021**, *143* (7), 2741–2750.

(3) Song, F.; Bai, L.; Moysiadou, A.; Lee, S.; Hu, C.; Liardet, L.; Hu, X. Transition Metal Oxides as Electrocatalysts for the Oxygen Evolution Reaction in Alkaline Solutions: An Application-Inspired Renaissance. *J Am Chem Soc* **2018**, *140* (25), 7748–7759.

(4) Soriano-López, J.; Musaev, D. G.; Hill, C. L.; Galán-Mascarós, J. R.; Carbó, J. J.; Poblet, J. M. Tetracobalt-Polyoxometalate Catalysts for Water Oxidation: Key Mechanistic Details. *J Catal* **2017**, *350*, 56–63.

(5) Yin, Q.; Tan, J. M.; Besson, C.; Geletii, Y. V; Musaev, D. G.; Kuznetsov, A. E.; Luo, Z.; Hardcastle, K. I.; Hill, C. L. A Fast Soluble Carbon-Free Molecular Water Oxidation Catalyst Based on Abundant Metals. *Science (1979)* **2010**, *328* (April), 342–345.

(6) Goberna-Ferrón, S.; Vigara, L.; Soriano-López, J.; Galán-Mascarós, J. R. Identification of a Nonanuclear $\{Co^{II}_9\}$ Polyoxometalate Cluster as a Homogeneous Catalyst for Water Oxidation. *Inorg Chem* **2012**, *51* (21), 11707–11715.

(7) Schiwon, R.; Klingan, K.; Dau, H.; Limberg, C. Shining Light on Integrity of a Tetracobalt-Polyoxometalate Water Oxidation Catalyst by X-Ray Spectroscopy before and after Catalysis. *Chem. Commun* **2014**, *50*, 100.

(8) Stracke, J. J.; Finke, R. G. Electrocatalytic Water Oxidation Beginning with the Cobalt Polyoxometalate $[Co_4(H_2O)_2(PW_9O_{34})_2]^{10-}$: Identification of Heterogeneous CoO_x as the Dominant Catalyst. *J Am Chem Soc* **2011**, *133* (38), 14872–14875.

(9) Stracke, J. J.; Finke, R. G. Water Oxidation Catalysis Beginning with 2.5 MM $[Co_4(H_2O)_2(PW_9O_{34})_2]^{10-}$: Investigation of the True Electrochemically Driven Catalyst at ≥600 MV Overpotential at a Glassy Carbon Electrode. *ACS Catal* **2013**, *3* (6), 1209–1219.

(10) Vickers, J. W.; Lv, H.; Sumliner, J. M.; Zhu, G.; Luo, Z.; Musaev, D. G.; Geletii, Y. V.; Hill, C. L. Differentiating Homogeneous and Heterogeneous Water Oxidation Catalysis: Confirmation That $[Co_4(H_2O)_2(\alpha\text{-}PW_9O_{34})_2]^{10-}$ Is a Molecular Water Oxidation Catalyst. *J Am Chem Soc* **2013**, *135* (38), 14110–14118.

(11) Folkman, S. J.; Soriano-Lopez, J.; Galán-Mascarós, J. R.; Finke, R. G. Electrochemically Driven Water-Oxidation Catalysis Beginning with Six Exemplary Cobalt Polyoxometalates: Is It Molecular, Homogeneous Catalysis or Electrode-Bound, Heterogeneous CoO_x Catalysis? *J Am Chem Soc* **2018**, *140* (38), 12040–12055.

(12) Folkman, S. J.; Finke, R. G. Electrochemical Water Oxidation Catalysis Beginning with Co(II) Polyoxometalates: The Case of the Precatalyst $Co_4V_2W_{18}O_{68}^{10-}$. *ACS Catal* **2017**, *7* (1), 7–16.

(13) Surendranath, Y.; Kanan, M. W.; Nocera, D. G. Mechanistic Studies of the Oxygen Evolution Reaction by a Cobalt-Phosphate Catalyst at Neutral PH. *J Am Chem Soc* **2010**, *132* (46), 16501–16509.

(14) Kanan, M. W.; Nocera, D. G. In Situ Formation of an Oxygen-Evolving Catalyst in Neutral Water Containing Phosphate and Co^{2+}. *Science (1979)* **2008**, *321* (5892), 1072–1075.

(15) Gao, D.; Trentin, I.; Schwiedrzik, L.; González, L.; Streb, C. The Reactivity and Stability of Polyoxometalate Water Oxidation Electrocatalysts. *Molecules* **2019**, *25* (1), 157.

(16) Lieb, D.; Zahl, A.; Wilson, E. F.; Streb, C.; Nye, L. C.; Meyer, K.; Ivanović-Burmazović, I. Water Exchange Reactivity and Stability of Cobalt Polyoxometalates under Catalytically Relevant PH Conditions: Insight into Water Oxidation Catalysis. *Inorg Chem* **2011**, *50* (18), 9053–9058.

(17) Borrás-Almenar, J. J.; Coronado, E.; Müller, A.; Pope, M. *Polyoxometalate Molecular Science*; Borrás-Almenar, J. J., Coronado, E., Müller, A., Pope, M., Eds.; Springer Netherlands: Dordrecht, 2003.

(18) Finke, R. G.; Droege, M. W.; Domaille, P. J. Trivacant Heteropolytungstate Derivatives. 3. Rational Syntheses, Characterization, Two-Dimensional ^{183}W NMR, and Properties of Tungstometallophosphates $P_2W_{18}M_4(H_2O)_2O_{68}^{10-}$ and $P_4W_{30}M_4(H_2O)_2O_{112}^{16-}$ (M = Co, Cu, Zn). *Inorg Chem* **1987**, *26* (23), 3886–3896.

(19) Galán-Mascarós, J. R.; Gómez-Garcia, C. J.; Borrás-Almenar, J. J.; Coronado, E. High Nuclearity Magnetic Clusters: Magnetic Properties of a Nine Cobalt Cluster Encapsulated in a Polyoxometalate, $[Co_9(OH)_3(H_2O)_6 (HPO_4)_2(PW_9O_{343}]^{16-}$. *Advanced Materials* **1994**, *6* (3), 221–223.

(20) Baumgärtel, N.; Flambard, A.; Köhler, F. H.; Lescouëzec, R. Paramagnetic Hexacyanometalates. The Diversity of Spin Distribution Studied by ^{13}C and ^{15}N MAS NMR Spectroscopy. *Inorg Chem* **2013**, *52* (21), 12634–12644.

(21) Vantelon, D.; Trcera, N.; Roy, D.; Moreno, T.; Mailly, D.; Guilet, S.; Metchalkov, E.; Delmotte, F.; Lassalle, B.; Lagarde, P.; Flank, A. M. The LUCIA Beamline at SOLEIL. *urn:issn:1600-5775* **2016**, *23* (2), 635–640.

(22) Ravel, B.; Newville, M. ATHENA, ARTEMIS, HEPHAESTUS: Data Analysis for X-Ray Absorption Spectroscopy Using IFEFFIT. *urn:issn:0909-0495* **2005**, *12* (4), 537–541.

(23) Mendoza, D.; Dong, S. T.; Kostopoulos, N.; Pinty, V.; Rivada-Wheelaghan, O.; Anxolabéhère-Mallart, E.; Robert, M.; Lassalle-Kaiser, B. In Situ X-Ray Absorption Spectroscopy in Homogeneous Conditions Reveals Interactions between CO_2 and a Doubly and Triply Reduced Iron(III) Porphyrin, Then Leading to Catalysis. *ChemCatChem* **2023**, *15* (7), e202201298.

(24) Nagaraja, C.; Venkatesha, T. V. The Influence of Electron Donating Tendency on Electrochemical Oxidative Behavior of Hydroquinone: Experimental and Theoretical Investigations. *Electrochim Acta* **2018**, *260*, 221–234.

(25) Goberna-Ferrón, S.; Soriano-López, J.; Galán-Mascarós, J. R.; Nyman, M. Solution Speciation and Stability of Cobalt-polyoxometalate Water Oxidation Catalysts by X-ray Scattering. *Eur J Inorg Chem* **2015**, *2015* (17), 2833–2840.

(26) Gumerova, N. I.; Rompel, A. Polyoxometalates in Solution: Speciation under Spotlight. *Chem Soc Rev* **2020**, *49* (21), 7568–7601.

(27) Reikowski, F.; Maroun, F.; Pacheco, I.; Wiegmann, T.; Allongue, P.; Stettner, J.; Magnussen, O. M. Operando Surface X-Ray Diffraction Studies of Structurally Defined Co_3O_4 and CoOOH Thin Films during Oxygen Evolution. *ACS Catal* **2019**, *9* (5), 3811–3821.

(28) Wiegmann, T.; Pacheco, I.; Reikowski, F.; Stettner, J.; Qiu, C.; Bouvier, M.; Bertram, M.; Faisal, F.; Brummel, O.; Libuda, J.; Drnec, J.; Allongue, P.; Maroun, F.; Magnussen, O. M. Operando Identification of the Reversible Skin Layer on Co_3O_4 as a Three-Dimensional Reaction Zone for Oxygen Evolution. *ACS Catal* **2022**, *12* (6), 3256–3268.

(29) Chivot, J.; Mendoza, L.; Mansour, C.; Pauporté, T.; Cassir, M. New Insight in the Behaviour of Co–H2O System at 25–150°C, Based on Revised Pourbaix Diagrams. *Corros Sci* **2008**, *50* (1), 62–69.

(30) Hall, M. D.; Underwood, C. K.; Failes, T. W.; Foran, G. J.; Hambley, T. W. Using XANES to Monitor the Oxidation State of Cobalt Complexes. *Aust J Chem* **2007**, *60* (3), 180–183.

(31) Wu, Q.; Xiao, M.; Wang, W.; Cui, C. In Situ Coordination Environment Tuning of Cobalt Sites for Efficient Water Oxidation. *ACS Catal* **2019**, *9* (12), 11734–11742.

(32) Singh, C.; Mukhopadhyay, S.; Das, S. K. Polyoxometalate-Supported Bis(2,2′-Bipyridine)Mono(Aqua)Nickel(II) Coordination Complex: An Efficient Electrocatalyst for Water Oxidation. *Inorg Chem* **2018**, *57* (11), 6479–6490.

(33) Yu, K.; Zhou, B. Bin; Yu, Y.; Su, Z. H.; Yang, G. Y. A New Organic-Inorganic Hybrid Layered Molybdenum(V) Cobalt Phosphate Constructed from $[H_{24}(Mo_{16}O_{32})Co_{16}(PO_4)_{24}(OH)_4(C_5H_4N)_2(H_2O)_6]^{4-}$ Wheels and 4,4′-Bipyridine Linkers. *Inorg Chem* **2011**, *50* (5), 1862–1867.

(34) Slesinski, A.; Sroka, S.; Fic, K.; Frackowiak, E.; Menzel, J. Operando monitoring of Local PH Value Changes at the varbon Electrode Surface in Neutral Sulfate-Based Aqueous Electrochemical. *ACS Appl Mater Interfaces* **2022**, *14* (33), 37782.

(35) Kuhn, A. T.; Chan, C. Y. PH Changes at Near-Electrode Surfaces. *J Appl Electrochem* **1983**, *13* (2), 189–207.

(36) Goberna-Ferrón, S.; Soriano-López, J.; Galán-Mascarós, J. R.; Nyman, M. Solution Speciation and Stability of Cobalt-polyoxometalate Water Oxidation Catalysts by X-ray Scattering. *Eur J Inorg Chem* **2015**, *2015* (17), 2833–2840.

(37) de Groot, F.; Vankó, G.; Glatzel, P. The 1s X-Ray Absorption Pre-Edge Structures in Transition Metal Oxides. *Journal of Physics: Condensed Matter* **2009**, *21* (10), 104207.

(38) Cabaret, D.; Bordage, A.; Juhin, A.; Arfaoui, M.; Gaudry, E. First-Principles Calculations of X-Ray Absorption Spectra at TheK-Edgeof 3dtransition Metals: An Electronic Structure Analysis of the Pre-Edge. *Physical Chemistry Chemical Physics* **2010**, *12* (21), 5502.

(39) Kuppuraj, G.; Dudev, M.; Lim, C. Factors Governing Metal-Ligand Distances and Coordination Geometries of Metal Complexes. *Journal of Physical Chemistry B* **2009**, *113* (9), 2952–2960.

(40) Blasco-Ahicart, M.; Soriano-López, J.; Carbó, J. J.; Poblet, J. M.; Galan-Mascaros, J. R. Polyoxometalate Electrocatalysts Based on Earth-Abundant Metals for Efficient Water Oxidation in Acidic Media. *Nat Chem* **2018**, *10* (1), 24–30.

(41) Vigara, L.; Carbó, J. J.; Soriano-López, J.; Galán-Mascarós, J. R.; Poblet, J. M.; Goberna-Ferrón, S. Cobalt Polyoxometalates as Heterogeneous Water Oxidation Catalysts. *Inorg Chem* **2013**, *52* (9), 4753–4755.

(42) Haider, A.; Bassil, B. S.; Soriano-López, J.; Qasim, H. M.; Sáenz De Pipaón, C.; Ibrahim, M.; Dutta, D.; Koo, Y. S.; Carbó, J. J.; Poblet, J. M.; Galán-Mascarós, J. R.; Kortz, U. 9-Cobalt(II)-Containing 27-Tungsto-3-Germanate(IV): Synthesis, Structure, Computational Modeling, and Heterogeneous Water Oxidation Catalysis. *Inorg Chem* **2019**, *58* (17), 11622–11629.

(43) Arens, J. T.; Blasco-Ahicart, M.; Azmani, K.; Soriano-López, J.; García-Eguizábal, A.; Poblet, J. M.; Galan-Mascaros, J. R. Water Oxidation Electrocatalysis in Acidic Media with Co-Containing Polyoxometalates. *J Catal* **2020**, *389*, 345–351.